Multipole moments and trap states in forward scattering of resonance light

Bogdan Łobodziński* and Wojciech Gawlik†
Instytut Fizyki Uniwersytetu Jagiellońskiego, ulica Reymonta 4, PL 30-059 Kraków, Poland
(Received 12 December 1995)

We perform nonperturbative analysis of forward scattering of resonance laser light on atoms in magnetic field when the laser drives transitions between states with total angular momenta $F=1,2$ and study the role of the induced higher-order multipole moments in the forward-scattering signal. It is shown how the multipole moments affect these signals and why not all possible multipoles are revealed for some transitions. The analysis is performed in terms of density-matrix formalism and in terms of coupled and uncoupled (trap) states. Evolution of the trap states in a magnetic field is found to be responsible for specific dependencies of the forward-scattering signals on the multipoles of various ranks. The general theory is applied to the case of the Na D_1 line. We also present a pump-probe method for studying multipoles in systems with states of high angular momenta and with complex transitions overlapping within their Doppler width. [S1050-2947(96)08108-5]

PACS number(s): 32.80.Bx, 33.55.Ad, 42.25.Bs

I. INTRODUCTION

One important consequence of atom-light interactions is induction of various multipole moments of the atomic electron distribution. Such multipoles are generally described in terms of irreducible tensor representation of the density matrix [1–3]. The tensorial components $\rho_q^{(k)}$ of the density matrix have a very simple physical interpretation: they are related to populations ($q=0$) and phase relations (coherences) of the specific atomic sublevels ($q\neq 0$) and could be easily associated with experimentally determined quantities. The $\rho_q^{(k)}$ components are also related to the density-matrix elements $\rho_{m,m'}$ in the $|L,m\rangle$ representation of atomic angular momentum in such a way that $q=\Delta m=m-m'$ and $|q|\leqslant k$ with $k\leqslant 2L$. The order of polarity of a given multipole moment is defined by its tensorial rank k as 2^k. Since $|q|\leqslant k$, only the coherences with maximum possible values of $\Delta m=q$, i.e., with $\Delta m=k$, can be associated with transverse components of a unique multipole while the coherences with $\Delta m<k$ are superpositions of components q of multipoles of various possible ranks. For instance, within $L=2$ and for linear light polarization, the possible ranks are $k=0,2,4$ and $\Delta m=q=0,\pm 2,\pm 4$. The population ($\Delta m=0$) consists then of contributions of longitudinal components of monopole $\rho_0^{(0)}$, quadrupole $\rho_0^{(2)}$, and hexadecapole $\rho_0^{(4)}$, the $\Delta m=2$ coherence consists of transverse components of quadrupole $\rho_{\pm 2}^{(2)}$ and hexadecapole $\rho_{\pm 2}^{(4)}$, and only the $\Delta m=4$ coherence is equivalent to a transverse component $\rho_{\pm 4}^{(4)}$ of a single multipole, the hexadecapole moment. In this paper we will therefore often use the notion of the hexadecapole moment or hexadecapole coherence, meaning the density-matrix element with $\Delta m=4$.

With a weak light intensity, such as in classical light sources, only single-photon couplings of atomic sublevels need to be considered. Because of the $\Delta m=0,\pm 1$ selection rules for electric dipole transitions between atomic states, only the sublevels of a given state with $|\Delta m|=|m-m'|\leqslant 2$ can be coupled by weak beams. Thus with weak light beams only quadrupole moments at most could be observed. The $|\Delta m|\leqslant 2$ restriction does not hold for strong, coherent light beams, in which case the Rabi frequency characterizing the light-atom interaction might exceed the homogeneous width of the perturbed transition. In such cases many photons are coherently exchanged in a sequence of absorptions and stimulated emissions (Rabi nutation) which couples the sublevels which may differ by any Δm allowed by quantum numbers of a given system. When the angular momenta of the states involved are sufficiently big, induction of multipole moments of higher orders ($k\geqslant 4$) is possible.

Evidence of such a quantity of $k>2$ was obtained in the experiment by Ducloy *et al.* [4]. In this work the hexadecapole moment ($k=4$) was detected in fluorescence light from a neon cell placed in a laser cavity in a magnetic field, i.e., in the nonlinear Hanle experiment [5]. The use of magnetic fields for studying the multipoles is possible because of their relation to magnetic sublevels. Another experiment where the light-induced multipole moments were reported was devoted to the study of forward scattering (FS) of resonance laser light by sodium atoms in a cell outside the laser cavity [6]. In this experiment, which was based on the nonlinear, resonant Faraday effect (NLFE), very strong nonlinear contributions to the Faraday rotation were attributed to the light-induced quadrupole and hexadecapole moments in the ground state of sodium atoms. Hexadecapole moments were also detected in experiments with fluorescence detection by Fischer and Hertel [7] and by McLean *et al.* [8]. An elegant way of studying the laser-induced multipole moments has been used by Suter *et al.* [9]. Using excitation modulated at a frequency of magnetic precession of a given multipole moment and phase-sensitive detection with Fourier analysis they could selectively detect multipoles of a given order. The method used by Yabuzaki *et al.* [10] where the Fourier analysis is applied to a broadband laser beam transmitted through an atomic vapor has similar potential. In both of these Fourier-transform experiments the amplitudes of the

*Electronic address: bogdan@castor.if.uj.edu.pl
†Electronic address: gawlik@castor.if.uj.edu.pl

possible hexadecapole contributions were, however, too small to be detected.

A full theoretical analysis of the forward-scattering experiments is very complicated for the case of strong lasers and transitions with hyperfine structure (hfs) and large angular momenta, because of the wealth of states and mutual couplings of their coherences and populations. For this reason the observations of FS signals by Gawlik *et al.* [6] remained without detailed, quantitative interpretation for a long time. An attempt to provide such an interpretation was made by Giraud-Cotton *et al.* [11], who performed perturbative, third-order calculations of the NLFE for the sodium lines with the aim of explaining the observations of Gawlik *et al.* Indeed, the calculated line shapes were qualitatively similar to some of the experimental ones reported in [6]. From this agreement, Giraud-Cotton *et al.* concluded that their perturbative analysis with only $\Delta m=2$ coherences, without invoking higher-order ($\Delta m=4$) ones, provides a satisfactory explanation. This started a long-lasting controversy, since as pointed out by Gawlik [12] the agreement was not exact and the theory of Giraud *et al.* was far from complete. In particular, the restoration of coherence and population by spontaneous emission was neglected in this treatment. Moreover, under the conditions of the experiment [6] substantial saturation made the perturbative approach inapplicable. On the other hand, the tentative interpretation of the results of Gawlik *et al.* apparently has not been sufficiently substantiated. In particular, the resemblance of their results to those reported by Ducloy is only superficial: the FS signals are not composed of peaks and dips that can be related to the specific multipole moments as in [4], rather they are superpositions of symmetrical contributions, all being zero at $B=0$. Amplitudes and widths of the contributions of various coherences have various intensity dependencies. As we will show below, this makes their unambiguous identification virtually impossible with a standard, single-beam arrangement.

Despite its deficiency, third-order perturbative analysis was performed by many authors, e.g., Jungner and coworkers [13] and Weis and co-workers [14]. These calculations included only quadrupolar coherences, yet they were in a good qualitative agreement with the experimental results even though the atomic states involved had sufficiently high angular momenta to allow the existence of higher multipoles. This agreement suggested that the possible hexadecapole coherence cannot produce dramatic changes of the signals obtained with single light beams, i.e., with the NLFE-FS arrangement, which has been convincingly demonstrated in a thorough recent experiment by Holmes and Griffith [15].

The surprising agreement of the experimental observations of FS by sodium atoms with a very simple theoretical description is an intriguing question that we wish to answer in this work. We will also show when, if at all, the hexadecapole moments can be observed in forward scattering of laser light and thereby solve the above-mentioned controversy.

Below we present detailed, nonperturbative analysis of the FS in the $|F,m\rangle$ representation, where F represents the angular momentum of a given hyperfine sublevel, and in terms of the coupled and uncoupled states in analogy with the phenomenon of the coherent-population trapping (CPT),

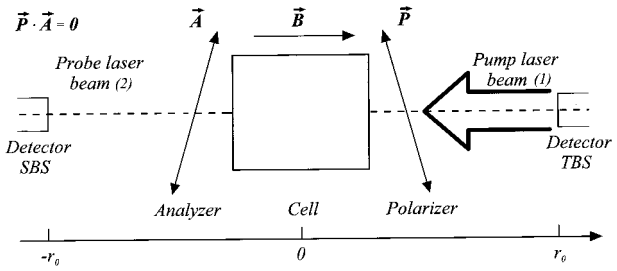

FIG. 1. Scheme of two geometries of the FS experiments considered in this paper. (i) SBS geometry where the same laser beam induces and probes multipole moments. For this geometry only beam (1) is used and FS signals are detected by the SBS detector at $-\mathbf{r}_0$. (ii) TBS geometry where the two roles are separated. The strong beam (1) induces the multipole moments which affect forward scattering of a weak, counterpropagating probe beam (2) of the same frequency. The probe FS signals are measured by the TBS detector at $\mathbf{r}_0$. **P** and **A** represent orientations of the polarizer and analyzer which are orthogonal to **B** and to themselves.

also related to laser-induced coherences [16]. While CPT is well known for the simple $J=0\leftrightarrow J=1$ and $J=1\leftrightarrow J=1$ systems, much less attention has been devoted to this phenomenon in more complex systems [17]. In this paper we also suggest a pump-probe approach to the studies of laser-induced multipole moments which should simplify identification of individual multipoles. Though the pump-probe arrangement has already been employed in the FS studies [9,18,19], here we analyze a geometry which allows sensitive detection of high-order multipoles with the velocity selection, i.e., sub-Doppler resolution, which is particularly useful for such complex systems as alkali-metal atoms. In Sec. II we specify two experimental arrangements for studies of FS: the standard single-beam scattering (SBS) and the alternative two-beam scattering (TBS) with a strong pump and a counterpropagating weak probe and present basic assumptions and definitions. In Sec. III we calculate the FS signals with the two geometries for the whole D_1 sodium line and for its various individual hfs components and we interpret the calculated signals in terms of the trap states in Sec. IV.

II. DESCRIPTION OF THE SYSTEM

A. Assumptions and definitions

In this paper we consider the experimental situation of the Faraday-effect geometry as depicted in Fig. 1. Atoms contained in a cell are placed within a constant, homogeneous magnetic field **B**. They can interact either with a single beam (SBS) or with two light beams counterpropagating along the direction of the field **B** (TBS). In the case of SBS a single beam (pump) induces coherences (multipoles) in the atomic sample and tests them as well, while in the case of TBS the coherences are induced by a strong pump beam (1) and are sampled by the weak probe beam (2). Both beams are linearly polarized perpendicularly to **B** (σ polarization) and beam 2 is detected after passing analyzer A crossed with polarizer P ($\mathbf{P}\cdot\mathbf{A}=0$). In that way only this part of the forward-scattering beam 2 is detected which undergoes polarization change while passing the atomic sample. If $B=0$

and no additional external perturbation is imposed on atoms, a single, linearly polarized light beam propagates through the vapor without any modification of its polarization. Thus no signal is seen by the detector due to symmetry between the $\sigma^{\pm}$ components of the propagating beam. If, however, either an additional light beam appropriately polarized (circularly or linearly with 45° with respect to **P** and **A**), or a longitudinal magnetic field is additionally perturbing the atoms, the $\sigma^{\pm}$ symmetry in the forward propagation of the probe is broken and there will be a nonzero signal after the crossed analyzer [20,21]. In the considered case the strong pump is linearly polarized in the direction perpendicular to the probe polarization, hence $B\neq 0$ is necessary to observe the forward-scattering signals with crossed polarizers. Since the multipole moments we are interested in are associated with the magnetic sublevels, they are affected by the magnetic field and correspondingly modify the forward-scattering signals, i.e., the dependencies of FS intensity on B.

We assume that both beams (pump and probe) are coherent fields of the same frequency ω_L. The positive frequency part of the total light field is

$$\mathbf{E}(\mathbf{r},t)=\{[\mathbf{A}E_1(\mathbf{r})]e^{i\mathbf{k}_1\cdot\mathbf{r}}+[\mathbf{P}E_2(\mathbf{r})]e^{i\mathbf{k}_2\cdot\mathbf{r}}\}e^{-i\omega_L t}, \quad (1)$$

where E_1 and E_2 are the amplitudes of the pump (1) and the probe (2) fields, while unit vectors **A**, **P** determine their polarizations and $\mathbf{k}_1=-\mathbf{k}_2$ (Fig. 1). We neglect any possible nonuniform transverse distribution of the incident light fields [22].

The field given by Eq. (1) interacts resonantly with atomic transition $F\leftrightarrow f$ where F and f are the total angular momenta of the upper and lower level, respectively. The $|F,m\rangle$ and $|f,\mu\rangle$ ($\mu=-f,\ldots,f$ and $m=-F,\ldots,F$) label corresponding Zeeman sublevels in the reference frame with quantization axis along **B**. Evolution of the density matrix describing our atomic system is governed by the master equation

$$\frac{d}{dt}\rho=-i[H,\rho]+\Lambda_R\rho+\Lambda_{\mathrm{coll}}\rho, \quad (2)$$

where H is the Hamiltonian of an atom in the magnetic field that interacts with two coherent fields and $\hbar=1$. The radiative relaxation ($\Lambda_R\rho$) due to spontaneous emission is considered in a standard way, see, e.g., [23]. The collisional relaxation ($\Lambda_{\mathrm{coll}}\rho$) is described within the impact limit and ignoring collisional shifts (we return to the case when collisions are important in Sec. III B) in a general way, allowing for different relaxation rates of various coherences. The relaxation terms are

$$\Lambda_R\rho=\gamma_e\sum_{l=1}^{N}\sum_{Fm,F'm'}\left(2\sum_{f\mu,f'\mu'}D^{f,F}_{\mu,m}\sigma^{(l)}_{f\mu,Fm}\times\rho D^{F',f'}_{m',\mu'}\sigma^{(l)}_{Fm',f'\mu'}-\{\sigma^{(l)}_{Fm,F'm'},\rho\}\right)-\gamma_g\sum_{l=1}^{N}\sum_{f\mu,f'\mu'}\{\sigma^{(l)}_{f\mu,f'\mu'},\rho\}, \quad (3)$$

$$\Lambda_{\mathrm{coll}}\rho=-\Gamma_1\sum_{l=1}^{N}\sum_{Fm}\sum_{f\mu}(\sigma^{(l)}_{Fm,Fm}\rho\sigma^{(l)}_{f\mu,f\mu}+\sigma^{(l)}_{f\mu,f\mu}\rho\sigma^{(l)}_{Fm,Fm})-\sum_{l=1}^{N}\sum_{Fm,F'm'}\sum_{f\mu,f'\mu'}(\sigma^{(l)}_{Fm,Fm}\rho\sigma^{(l)}_{F'm',F'm'}+\sigma^{(l)}_{f\mu,f\mu}\rho\sigma^{(l)}_{f'\mu',f'\mu'})[\Gamma_0\delta_{F'\neq F}+\Gamma_2(\delta_{f,f'}\delta_{\mu',\mu\pm2}+\delta_{F,F'}\delta_{m',m\pm2})+\Gamma_4(\delta_{f,f'}\delta_{\mu',\mu\pm4}+\delta_{F,F'}\delta_{m',m\pm4})].$$

In (3) γ_e stands for relaxation (spontaneous emission) rate of the upper state, γ_g is the transit relaxation rate of the lower (ground) state, $\{\ \}$ denotes the anticommutator, e.g., $\{A,B\}=AB+BA$, while Γ_r ($r=0,1,2,4$) are the collisional relaxation rates of optical coherences ($r=1$), hyperfine coherences ($F\neq F'$, $r=0$), quadrupole coherences ($F=F'$, $m'=m\pm2$, $r=2$), and hexadecapole coherences ($F=F'$, $m'=m\pm4$, $r=4$), and $\delta_{m',m\pm r}$ is the Kronecker delta. $\sigma^{(l)}_{Fm,f\mu}=|F,m\rangle_l\langle f,\mu|_l$ is the atomic coherence operator of atom l. $D^{F,f}_{m,\mu}$ describe the angular part of the $\mathbf{D}^{F,f}_{m,\mu}=\langle F,m|\mathbf{D}|f,\mu\rangle$ matrix elements. For the assumed geometry ($\mathbf{A}\cdot\mathbf{P}=0$) we have

$$\mathbf{D}^{F,f}_{m,\mu}\cdot\mathbf{P}=iD^{F,f}_{m,\mu}d_{F,f},$$

$$\text{then}\ \ \mathbf{D}^{F,f}_{m,\mu=m\pm1}\cdot\mathbf{A}=\pm D^{F,f}_{m,\mu=m\pm1}d_{F,f}, \quad (4)$$

where $d_{F,f}=\langle F||d||f\rangle$ stands for the reduced matrix element. With the above definitions, making the standard rotating-wave approximation and assuming optically thin medium and weak magnetic field, the full Hamiltonian can be obtained by summing individual Hamiltonians $H=H_A+H_1+H_2$ describing the atoms in the magnetic field (H_A) and interacting with two coherent fields (H_1,H_2),

$$H_A=\sum_{l=1}^{N}\left[\sum_{Fm,Fm'}\sigma^{(l)}_{Fm,Fm'}(\omega_0^F+m\omega_B g_F)+\sum_{f\mu,f\mu'}\sigma^{(l)}_{f\mu,f\mu'}(\omega_0^f+\mu\omega_B g_f)\right], \quad (5)$$

$$H_1=i\sum_{l=1}^{N}\left[\sum_{F,m}\sum_{f,\mu}\Omega_1^{F,f}(D^{F,f}_{m,\mu}e^{i\mathbf{k}_1\cdot\mathbf{r}_l}\sigma^{(l)}_{Fm,f\mu}-D^{f,F}_{\mu,m}e^{-i\mathbf{k}_1\cdot\mathbf{r}_l}\sigma^{(l)}_{f\mu,Fm})\right], \quad (6)$$

and

$$H_2=-\sum_{l=1}^{N}\left(\sum_{F,m}\sum_{f,\mu}\Omega_2^{F,f}[D^{F,f}_{m,\mu}e^{i\mathbf{k}_2\cdot\mathbf{r}_l}(\sigma^{(l)}_{Fm,f\mu}\delta_{\mu,m-1}-\sigma^{(l)}_{Fm,f\mu}\delta_{\mu,m+1})+D^{f,F}_{\mu,m}e^{-i\mathbf{k}_2\cdot\mathbf{r}_l}(\sigma^{(l)}_{f\mu,Fm}\delta_{\mu,m-1}-\sigma^{(l)}_{f\mu,Fm}\delta_{\mu,m+1})]\right), \quad (7)$$

where ω_0^F and ω_0^f are the energies ($\hbar=1$) of the upper (F) and lower (f) states of the $F\leftrightarrow f$ transition for $B=0$, ω_L is the laser frequency, $\omega_B=\mu_B B$ is the Larmor frequency (μ_B being the Bohr magneton), $g_F(g_f)$ are the Landé factors of the $F(f)$ states, and $\Omega_j^{F,f}=E_j d_{F,f}$ ($j=1,2$) is the Rabi frequency associated with field $\mathbf{E}_j$ and the $F\leftrightarrow f$ transition.

In this work we do not differentiate between relaxation rates of multipoles of various ranks within the given state except when we assume very rapid relaxation of the hexadecapole coherences to study their specific effect on the FS signals. As a matter of fact, such differentiation would not be possible within the $|F,m\rangle$ representation. We have, nevertheless, chosen this basis since it allows easier interpretation of the light-induced coherences and their relation to the trapped states.

B. Experimental situation

Now, we consider the following two specific cases of the scattering of the single strong beam only or of the weak probe in the presence of a counterpropagating pump.

1. Single-beam forward scattering

In this section we investigate an experimental situation without a weak beam ($E_2=0$), i.e., when a single strong beam generates and probes the coherences. To take fully into account the coherent character of FS we express the positive frequency part of the operator of the electric field radiated by the ensemble of N atoms and seen by the SBS detector after passing analyzer $\mathbf{A}$ (Fig. 1) by

$$E_{\mathrm{SBS}}^{(+)}\left(-\mathbf{r}_0,t+\frac{r_0}{c}\right)=-ig\sum_{l=1}^{N}\sum_{Fm,f\mu}(\mathbf{A}\cdot\mathbf{D}_{m,\mu}^{F,f})\times\sigma_{Fm,f\mu}^{(l)}e^{-i(\omega_L t-\mathbf{k}_1\cdot\mathbf{r}_0)},\tag{8}$$

where g is a constant and $-\mathbf{r}_0$ is the detector position. The coherent nature of SBS is reflected in the above equation by the fact that the total field in the forward direction does not depend on positions of individual atoms [20,24,25]. For crossed P and A only field (8) reaches the detector and the intensity of the forward scattering is

$$\begin{aligned}I_{\mathrm{SBS}}&\left(-\mathbf{r}_0,t+\frac{r_0}{c}\right)\\&=g^2(N-1)N\sum_{F,f}\sum_{F',f'}\sum_{m,\mu}\sum_{m',\mu'}(\mathbf{A}\cdot\mathbf{D}_{m,\mu}^{F,f})\\&\quad\times(\mathbf{D}_{\mu',m'}^{f',F'}\cdot\mathbf{A})\langle\sigma_{Fm,f\mu}^{(1)}(t)\sigma_{f'\mu',F'm'}^{(2)}(t)\rangle_{\mathrm{av}}\\&\quad+g^2N\sum_{F,F'}\sum_{m,m'}\sum_{\mu}(\mathbf{A}\cdot\mathbf{D}_{m,\mu}^{F,f})(\mathbf{D}_{\mu,m'}^{f,F'}\cdot\mathbf{A})\\&\quad\times\langle\sigma_{Fm,F'm'}^{(1)}(t)\rangle_{\mathrm{av}}.\end{aligned}\tag{9}$$

By $\langle\ \rangle_{\mathrm{av}}$ we denote averages over the laser field fluctuations, over the density matrix of the system, and over atomic thermal velocities. As usual, $N\gg1$ and the first term in the above expression dominates the scattering signal. This is the typical coherent FS signal which, in general, depends on two-atom averages. The second term in (9) depends on Zeeman and hyperfine coherences. Though negligible in forward direction, it becomes relevant in lateral scattering [24] (it is this term that is responsible for such single-atom interference effects as the Hanle effect in fluorescence light [5]).

We calculate the FS signals according to (9) for transitions with $F,f=1,2$ making several simplifying assumptions. First, we assume that the incident field E_1 is coherent. This allows decorrelating two-atom averages in (9) which is a substantial simplification, not permissible in general but possible with a coherent field:

$$\langle\sigma_{Fm,f\mu}^{(1)}(t)\sigma_{f'\mu',F'm'}^{(2)}(t)\rangle_{\mathrm{av}}=\langle\sigma_{Fm,f\mu}^{(1)}(t)\rangle_{\mathrm{av}}\langle\sigma_{f'\mu',F'm'}^{(2)}(t)\rangle_{\mathrm{av}}.\tag{10}$$

Nonperturbative analysis of the SBS signals for various light statistics and for a simple $F=1\leftrightarrow f=0$ transition was performed in [26]. Secondly, we neglect the hyperfine coherences. This assumption is realistic when the Rabi frequency $\Omega_1^{F,f}$ is smaller than hfs of the levels involved in the considered transition. The next simplification concerns averaging over the Maxwell distribution of atomic velocities. Because the FS signal decreases fast with the detuning of laser frequency from the atomic resonance, the total FS field can be taken as a sum over these atomic transitions for which the Doppler shifted frequencies are in resonance with ω_L. This allows us to calculate the radiated field (8) as a simple sum of the contributions corresponding to resonant excitation of the hfs components $F\leftrightarrow f$ of the given line with appropriate Doppler weights $e^{-[(\omega_L-\omega_0^F+\omega_0^f)/\Delta\omega]^2}$, where $\Delta\omega$ is the Doppler width. However, nonresonant transitions can be very important for the dynamics of a given density element. We therefore calculate the optical coherences entering (8) by taking into account all nonresonant components in the master equation (2).

2. Two-beam forward scattering

In this subsection we consider the situation when two different beams, strong pump (1) for creation and weak probe (2) for detection of atomic coherences, are used. Similarly to the SBS case, the total electric field radiated by N atoms and observed behind the polarizer P by the TBS detector can be expressed as

$$E_{\mathrm{TBS}}^{(+)}\left(\mathbf{r}_0,t+\frac{r_0}{c}\right)=-ig\sum_{l=1}^{N}\sum_{Fm,f\mu}(\mathbf{P}\cdot\mathbf{D}_{m,\mu}^{F,f})\times\sigma_{Fm,f\mu}^{(l)}e^{-i[\omega_L t-\mathbf{k}_2\cdot(\mathbf{r}_l-\mathbf{r}_0)]}.\tag{11}$$

In contrast to the SBS case, we have to fully account for the different phases of the pump and probe beams at the position of each atom, which results in the following expression for the FS intensity of the probe beam:

$$
\begin{aligned}
&I_{\mathrm{TBS}}\left(\mathbf{r}_0,t+\frac{r_0}{c}\right)\\
&\quad=g^2\sum_{l=1}^{N}\sum_{j\neq l}^{N}\sum_{F,f}\sum_{F',f'}\sum_{m,\mu}\sum_{m',\mu'}(\mathbf{P}\cdot\mathbf{D}^{F,f}_{m,\mu})(\mathbf{D}^{f',F'}_{\mu',m'}\cdot\mathbf{P})\\
&\quad\times\langle\sigma^{(j)}_{Fm,f\mu}(t_j)\sigma^{(l)}_{f'\mu',F'm'}(t_l)\rangle_{\mathrm{av}}e^{-i\mathbf{k}_2\cdot(\mathbf{r}_j-\mathbf{r}_l)}\\
&\quad+g^2\sum_{l=1}^{N}\sum_{F,F',f}\sum_{m,m'}\sum_{\mu}(\mathbf{P}\cdot\mathbf{D}^{F,f}_{m,\mu})\\
&\quad\times(\mathbf{D}^{f,F'}_{\mu,m'}\cdot\mathbf{P})\langle\sigma^{(l)}_{Fm,F'm'}(t_l)\rangle_{\mathrm{av}},
\end{aligned}
\tag{12}
$$

where $t_l=r_l/c$. Weak intensity of the probe beam allows expansion of the averaged density-matrix elements to the first order in E_2 but to all orders in E_1:

$$
\begin{aligned}
\langle\sigma^{(l)}_{Fm,f\mu}(t_l)\rangle_{\mathrm{av}}&=\rho_{Fm,f\mu}e^{i\mathbf{k}_1\cdot\mathbf{r}_l}+\delta\rho^{(l)}_{Fm,f\mu}e^{i\mathbf{k}_2\cdot\mathbf{r}_l},\\
\langle\sigma^{(l)}_{f\mu,f'\mu'}\rangle_{\mathrm{av}}&=\rho^{(l)}_{f\mu,f'\mu'}+\delta\rho^{(l)}_{f\mu,f'\mu'}(t_l),\\
\langle\sigma^{(l)}_{Fm,F'm'}\rangle_{\mathrm{av}}&=\rho^{(l)}_{Fm,F'm'}+\delta\rho^{(l)}_{Fm,F'm'}(t_l),
\end{aligned}
\tag{13}
$$

where the ρ elements depend only on the pump field strength (to all orders) just as in the SBS case, whereas $\delta\rho$'s describe contributions due to the probe field to the first order in E_2 (and to all orders in E_1). With such an approach and with the assumption that the light fields are coherent, allowing the decorrelation of two-atom averages, the total intensity of the TBS signal can be written as

$$
\begin{aligned}
I_{\mathrm{TBS}}\left(\mathbf{r}_0,t+\frac{r_0}{c}\right)&=g^2\sum_{l}^{N}\sum_{j\neq l}^{N}\sum_{F,f}\sum_{F',f'}\sum_{m,\mu}\sum_{m',\mu'}(\mathbf{P}\cdot\mathbf{D}^{F,f}_{m,\mu})(\mathbf{D}^{f',F'}_{\mu',m'}\cdot\mathbf{P})[\,\delta\rho^{(j)}_{Fm,f\mu}\rho_{f'\mu',F'm'}e^{-i(\mathbf{k}_1-\mathbf{k}_2)\cdot\mathbf{r}_j}\\
&\quad+\rho_{Fm,f\mu}\delta\rho^{(l)}_{f'\mu',F'm'}e^{i(\mathbf{k}_1-\mathbf{k}_2)\cdot\mathbf{r}_l}+\rho_{Fm,f\mu}\rho_{f'\mu',F'm'}e^{i(\mathbf{k}_1-\mathbf{k}_2)(\mathbf{r}_j-\mathbf{r}_l)}+\delta\rho^{(k)}_{Fm,f\mu}\delta\rho^{(l)}_{f'\mu',F'm'}]\\
&\quad+g^2\sum_{l}^{N}\sum_{F,F',f}\sum_{m,m'}\sum_{\mu}(\mathbf{P}\cdot\mathbf{D}^{F,f}_{m,\mu})(\mathbf{D}^{f,F'}_{\mu,m'}\cdot\mathbf{P})[\rho_{Fm,f\mu}\delta\rho^{(l)}_{f\mu,F'm'}e^{i(\mathbf{k}_1-\mathbf{k}_2)\cdot\mathbf{r}_l}\\
&\quad+\delta\rho^{(l)}_{Fm,f\mu}\rho_{f\mu,F'm'}e^{-i(\mathbf{k}_1-\mathbf{k}_2)\cdot\mathbf{r}_l}+\rho_{Fm,F'm'}+\delta\rho^{(l)}_{Fm,f\mu}\delta\rho^{(l)}_{f\mu,F'm'}]\,.
\end{aligned}
\tag{14}
$$

From now on we leave out atomic labeling in the ρ elements because to the zeroth order in E_2 the solutions of the Bloch equations with a single field E_1 do not depend on atomic positions. On the contrary, such a dependence exists in $\delta\rho$'s and some of the terms in (14) cancel out after the summation over statistical atomic positions. Finally, after neglecting the terms linear in N, a simple formula for the TBS signal is obtained:

$$
\begin{aligned}
I_{\mathrm{TBS}}\left(\mathbf{r}_0,t+\frac{r_0}{c}\right)&=g^2\sum_{l}^{N}\sum_{j\neq l}^{N}\sum_{F,F'}\sum_{f,f'}\sum_{m,m'}\sum_{\mu,\mu'}(\mathbf{P}\cdot\mathbf{D}^{F,f}_{m,\mu})\\
&\quad\times(\mathbf{D}^{f',F'}_{\mu',m'}\cdot\mathbf{P})\,\delta\rho^{(j)}_{Fm,f\mu}\delta\rho^{(l)}_{f'\mu',F'm'}\,.
\end{aligned}
\tag{15}
$$

An important consequence of using two counterpropagating beams of the same frequency is Doppler-free selection of a specific hfs component of a complex transition, which makes Doppler averaging superfluous. Selection of a given hfs component allows neglecting of other hfs states (f,f' and F,F') in the net TBS signal (15) and writing it in a simplified form without summation over all F,F',f,f':

$$
\begin{aligned}
I_{\mathrm{TBS}}\left(\mathbf{r}_0,t+\frac{r_0}{c}\right)&\approx g^2\sum_{m,m'}\sum_{\mu,\mu'}(\mathbf{P}\cdot\mathbf{D}^{F,f}_{m,\mu})(\mathbf{D}^{f',F'}_{\mu',m'}\cdot\mathbf{P})\\
&\quad\times\delta\rho_{Fm,f\mu}\delta\rho_{f'\mu',F'm'},
\end{aligned}
\tag{16}
$$

where collective, position-averaged quantities $\delta\rho_{Fm,f\mu}=\Sigma_l\delta\rho^{(l)}_{Fm,f\mu}$ are introduced. However, the $\delta\rho$ elements in (15) and (16) are calculated taking all components, including the nonresonant ones, into account in Eq. (2) with substitutions (13). Detailed discussion of the equations for the collective variables $\delta\rho$ and their solutions is presented in the Appendix.

III. CALCULATED SIGNALS

A. SBS signals

In this section we present FS signals calculated for various specific atomic transitions and the SBS geometry (the case of TBS will be discussed in Sec. III B). We performed the calculations with atomic constants (hfs, relaxation rates, dipole moments) corresponding to the sodium D_1 line ($3\,^2S_{1/2}$–$3\,^2P_{1/2}$) for a comparison with the experimental results of Ref. [6]. In particular, we take $\gamma_e=(2\pi\tau)^{-1}$ (with $\tau=16$ ns being the radiative lifetime of the sodium excited $3\,^2P_{3/2}$ state) as a common relaxation rate of populations and Zeeman coherences off all upper-state magnetic sublevels and $\gamma_g=2\pi\times0.3$ MHz as a common lower-state relaxation rate related to a typical atomic transit time across the laser beam. In our calculations we take the values of the Rabi frequency below $2\pi\times60$ MHz which is sufficiently smaller than the $2\pi\times189$ MHz hyperfine splitting of the $^3P_{1/2}$ excited state to justify neglecting the hyperfine coherences.

The main purpose of these calculations was to observe to what extent the multipoles of the highest possible rank, i.e., the hexadecapole moments for $F,f=2$, affect the FS signals.

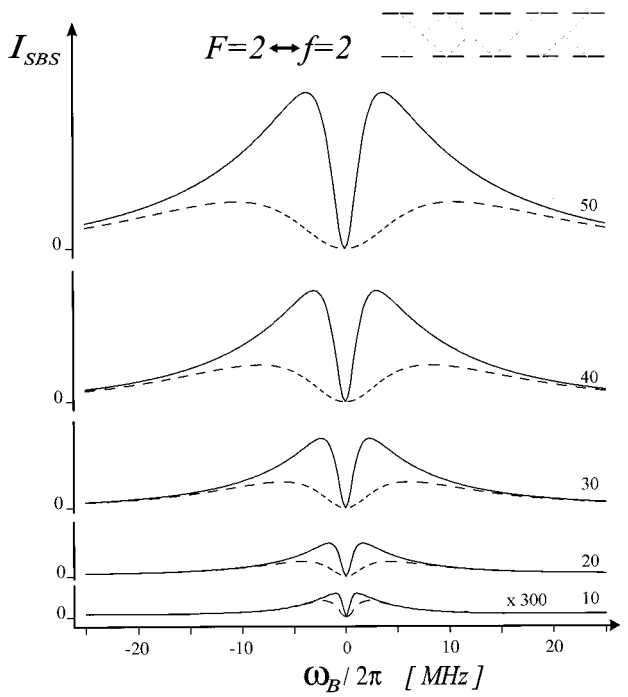

FIG. 2. SBS signals simulated for the single $F=2\leftrightarrow f=2$ transition and for various Rabi frequencies (Ω_0) marked on the right wing of each curve. Purely radiative relaxation is assumed, i.e., relaxation rate of optical coherences $\gamma_{\rm coh}=(\gamma_e+\gamma_g)/2$ and $\gamma_e=2\pi\times 10$ MHz, $\gamma_g=2\pi\times 0.3$ MHz. Solid lines represent the signals calculated with all possible coherences and the dashed lines are used for the signals without the hexadecapole moments.

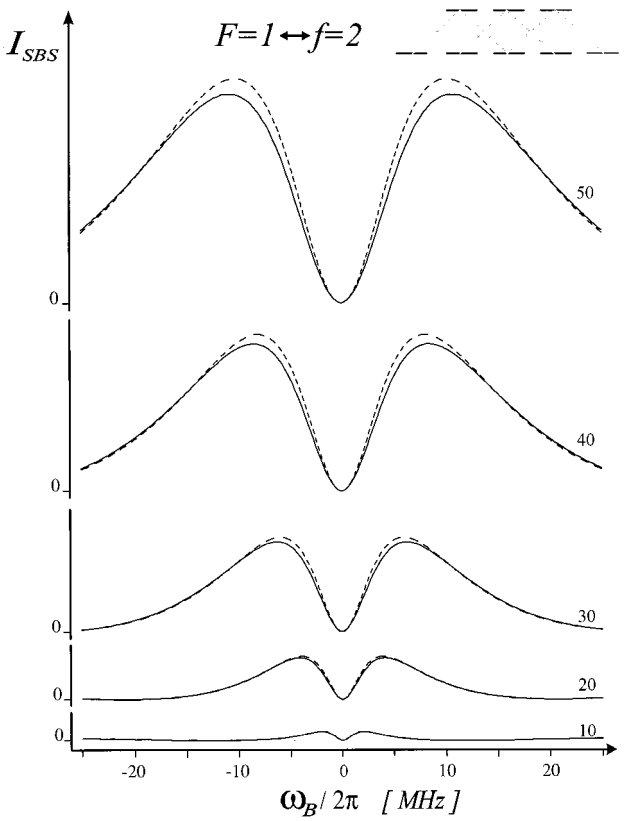

FIG. 3. SBS signals simulated for the single $F=1\leftrightarrow f=2$ transition. All parameters are the same as in Fig. 2.

We adopt the same method as used by McLean *et al.* [8], i.e., we calculate the signals with the hexadecapole moments (coherences $\rho_{-2,+2}$) properly included in the equations and with these moments quenched by assuming their very fast relaxation rates. Comparison of the signals calculated with and without the hexadecapole moments allows direct evaluation of the role of such multipoles in the FS. We first analyzed the SBS signals for well resolved single transitions between levels of total angular momenta $F,f=1,2$. By considering single transitions we were not restricted to closed atomic systems so, unlike Refs. [11,14], we could properly account for redistribution of population and coherences by spontaneous emission within, as well as out of, the initial system. Having analyzed the effect of the higher-order multipoles on the SBS signals with single transitions we then study their effect on complex transitions involving several, not necessarily resolved, components, e.g., hfs. As a representative example we take here the Na D_1 line.

1. Single transitions

Figures 2–5 illustrate velocity-averaged (as described in Sec. II B 1) SBS signals for single transitions: $F=2\leftrightarrow f=2$, $F=1\leftrightarrow f=2$, $F=2\leftrightarrow f=1$, and $F=1\leftrightarrow f=1$. Their common features are zero values of the FS intensity at $\omega_B=0$ when perfectly crossed polarizers are used and characteristic, two-peaked shapes resembling a squared dispersion function, symmetric around $\omega_B=0$. Strongly simplifying, by neglecting magnetic dependence of the optical coherences, each Zeeman coherence could be associated with a separate resonance contribution of the width (defined by the turning points of each squared dispersive line shape) determined by $\gamma/\Delta m$, where γ is the relaxation rate of a given state (γ_e or γ_g) and Δm denotes the difference of magnetic quantum numbers associated with the coherence

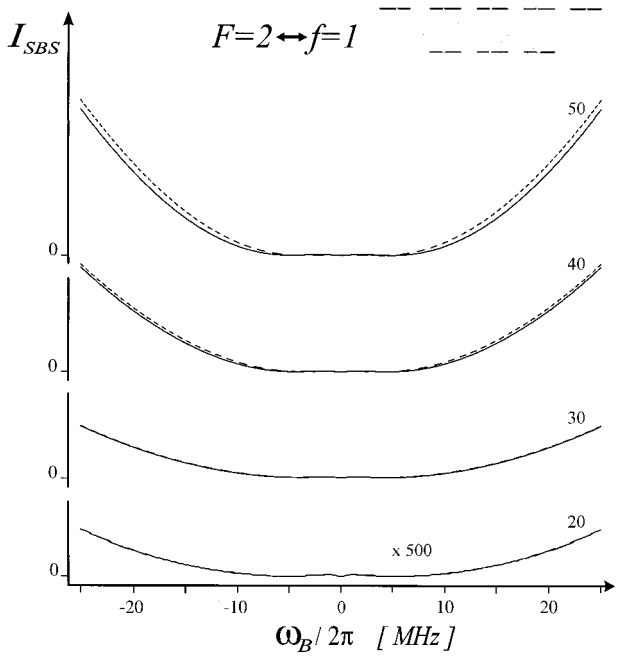

FIG. 4. SBS signals simulated for the single $F=2\leftrightarrow f=1$ transition. All parameters are the same as in Fig. 2.

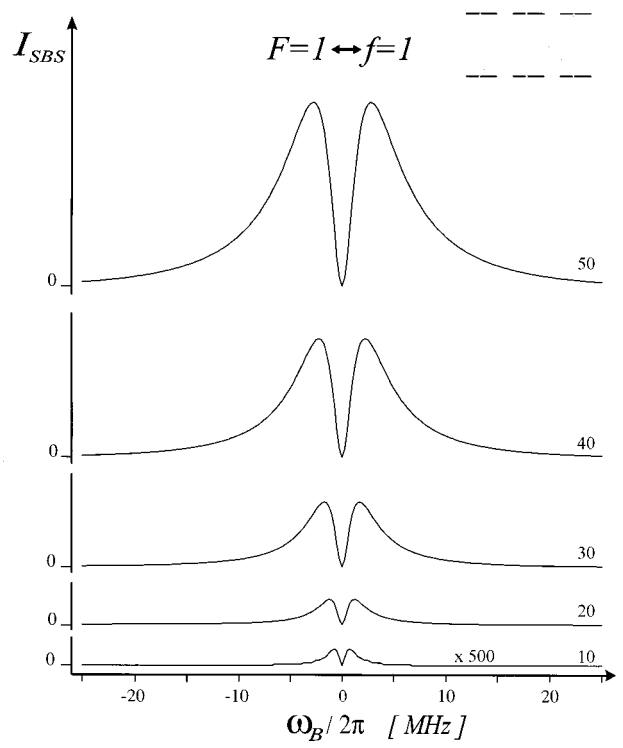

FIG. 5. SBS signals simulated for the single $F=1\leftrightarrow f=1$ transition. All parameters are the same as in Fig. 2. There are only solid lines as no hexadecapole contributions are possible for this transition.

considered. In that way individual contributions of each coherence should be easily recognizable in the net FS signal, provided γ_e and γ_g differ sufficiently. In practice, however, such a distinction is not that easy, on the one hand, because of the magnetic dependence of optical coherences which also contribute to the FS signals and, on the other hand, due to power broadening which affects various coherences in various degrees. In consequence, it is relatively easy to distinguish the lower-state multipoles from those of the upper state if one of the levels is long lived, e.g., the ground state as in the case we are interested in, but it is not possible in general to observe clearly resolved quadrupole and hexadecapole resonances within the same state except of some special cases shown below.

Figures 2–4 correspond to transitions where hexadecapole moments can be generated at least in one of the states, whereas for the transition $F=1\leftrightarrow f=1$, associated with Fig. 5, the highest possible multipoles are quadrupoles. The solid lines depict signals calculated with all possible coherences while the broken lines are signals obtained after elimination of the hexadecapole coherences $\rho_{-2,+2}$ (in both states). Within the range of ω_B spanned in Figs. 2–5, we see essentially only the ground-state multipoles.

As shown in Fig. 2, the effect of the ground-state hexadecapole moment on the SBS signals is very strong in the case of the $F=2\leftrightarrow f=2$ transition. After elimination of the hexadecapoles the signals are dominated by the ground-state coherences with $\Delta m=2$ (quadrupoles) and are clearly broader (by nearly a factor of 2 as expected from the ratio of the Δm values).

The very spectacular manifestation of the laser-induced hexadecapole moment, as seen in Fig. 2, is by no means a general feature of the SBS signals. For different transitions with $f,F=1,2$ the results are quite different. In Fig. 3 we show the SBS signals for the single $F=1\leftrightarrow f=2$ transition. There is only a small difference between the dashed and solid curves, i.e., the hexadecapole contributions to the SBS signal are hardly visible although this moment can be induced in the $f=2$ ground state. The main contribution to the SBS signal for the $F=1\leftrightarrow f=2$ transition is brought by the quadrupole coherences in the ground state. This behavior, dramatically different from the $F=2\leftrightarrow f=2$ case, is very interesting since the $F=1\leftrightarrow f=2$ energy-level structure has often been considered as the model structure for the analysis of the hexadecapole moments [3]. An additional unexpected feature of the SBS signals for the $F=1\leftrightarrow f=2$ transition is a slightly narrower structure for the case when the hexadecapole moment is eliminated than when it is included. The SBS signals calculated for the $F=2\leftrightarrow f=1$ transition are present in Fig. 4. Differences between the cases with and without hexadecapole are again hardly visible, which is easy to understand since for this transition the hexadecapole occurs only in the upper state. The slight divergence between the solid and dashed curves, seen for greater Rabi and Larmor frequencies, is mainly due to the upper-state hexadecapole.

The SBS signals for the $F=1\leftrightarrow f=1$ component (Fig. Fig. 5) are very similar to those for the $F=2\leftrightarrow f=2$ transition despite the fact that no hexadecapole coherence can be induced in either of the states $f,F=1$. The depicted signals are mainly due to the quadrupole moments in the ground state $f=1$. This similarity between the transitions $F=2\leftrightarrow f=2$ and $F=1\leftrightarrow f=1$ caused many incorrect interpretations in the previous literature. We wish to stress here the fact that despite this similarity the signals corresponding to the $F=2\leftrightarrow f=2$ transition cannot be correctly described within the third-order perturbation theory.

2. Complex transitions

As an example of a complex transition we examine the D_1 sodium line which consists of four hfs components; each of them has been analyzed above as a single transition. We do not consider the D_2 ($3\,^2S_{1/2}$–$3\,^2P_{3/2}$) transition here since its detailed analysis is much more complex because of the wealth of relevant atomic states (the excited state of $J=3/2$ has four hfs sublevels $F=0,1,2,3$) and is by no means more instructive than the D_1 line. However, in the case of overlapping components, such calculations require not only summation of individual components and velocity averaging but also taking into account the mutual influence of various transitions. The resulting SBS signals are presented in Fig. 6. We calculated these signals for ω_L tuned to the center-of-gravity frequency of the D_1 line using our Doppler-averaging method, described in Sec. II B 2. Similar results are obtained when the laser frequency is varied over the range comparable with hfs of the upper state, one order of magnitude smaller than the Doppler width. As before, the solid lines represent the signals calculated with all possible coherences and the dashed lines are used for the signals without the hexadecapole moments in both states ($3\,^2S_{1/2}$ and $3\,^2P_{1/2}$). In order to see the upper-state contributions to the FS signals for the whole D_1 line, in Fig. 6 we extended the range of ω_B with

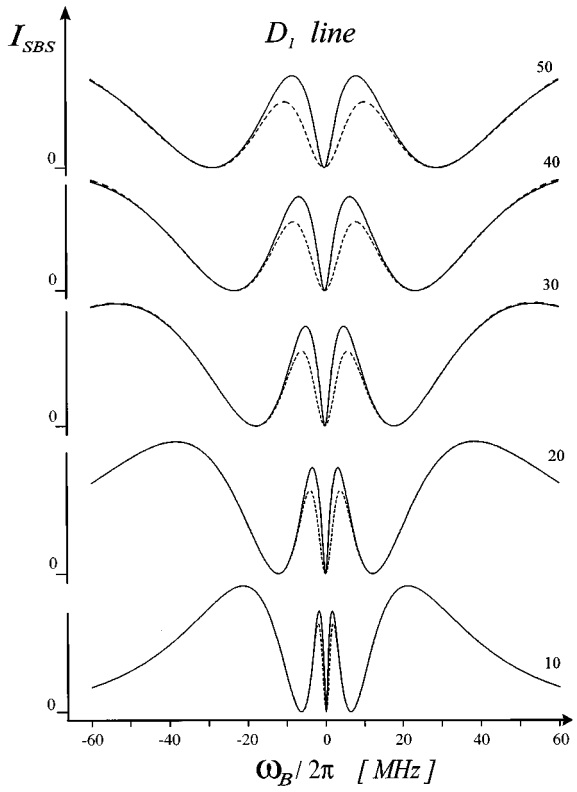

FIG. 6. SBS signals simulated for the whole Na D_1 line with Doppler averaging. All other parameters are as in Fig. 2. Solid lines represent signals with hexadecapole moments and dashed lines show the signals without the hexadecapoles.

respect to the previous figures. As can be seen, in the range of $|\omega_B| \leqslant 2\pi \times 20$ MHz, the resulting signals depend very little on the hexadecapole moment. They are most similar to those of Fig. 3 associated with a single $F=1 \leftrightarrow f=2$ transition with nearly no hexadecapole contribution. Though the $F=1 \leftrightarrow f=2$ and $F=2 \leftrightarrow f=2$ hfs components contribute with the same strengths to the D_1 line, the latter component (which, as shown in Fig. 2, has a very pronounced hexadecapole contribution) has very little impact on the net FS signal. The amplitude of the $F=2 \leftrightarrow f=2$ contribution to the signal for the entire D_1 line, B_{22}, is about one order of magnitude smaller than the amplitude B_{12} associated with the $F=1 \leftrightarrow f=2$ component. For instance, for $\Omega_0=2\pi \times 40$ MHz we have $B_{22}/B_{12}=0.13$. Also the $F=2 \leftrightarrow f=1$ component does not contribute much to the signals in a narrow range of $|\omega_B| \leqslant 2\pi \times 20$ MHz and is responsible mainly for the broad structure of the signals in Fig. 6 and the component $F=1 \leftrightarrow f=1$ is negligible: $B_{11}/B_{12}=0.007$.

The fact that the net signals calculated nonperturbatively for the whole Na D_1 line with all possible multipoles are dominated by the individual hfs component $F=1 \leftrightarrow f=2$ with negligible hexadecapole contribution explains the good agreement between the experimental results [6] and previous third-order calculations [11,13,15], by definition restricted to the quadrupole coherences.

B. TBS signals

To calculate the TBS signals according to (16) one has to find the collective variables $\delta\rho_{Fm,f\mu}$. They can be obtained

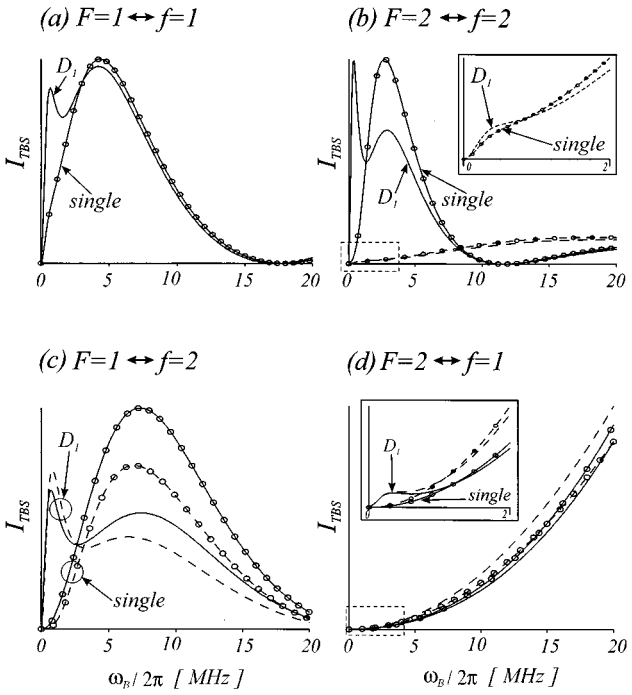

FIG. 7. The TBS signals calculated for different individual components of the D_1 sodium line. (The curves are symmetric around $\omega_B=0$.) $\Omega_0=2\pi \times 45$ MHz and relaxation rates are the same as in Fig. 2. The solid and broken lines represent the signals with Doppler-free selection of a given $F \leftrightarrow f$ hfs component from the whole Na D_1 line, whereas the dotted lines refer to single transitions $F \leftrightarrow f$. The solid (broken) lines refer to signals with (without) hexadecapoles. The insets for $F=2 \leftrightarrow f=2$ and $F=2 \leftrightarrow f=1$ transitions show enlargement of the marked region of small Larmor frequencies (the inset for $F=2 \leftrightarrow f=2$ shows only signals without hexadecpole moments).

by solving Eq. (2) with substitutions (13) which, under steady-state conditions and after position integration, yields the following equation (see the Appendix for more details):

$$i \sum_{F',f'} \Omega_2^{f',F'} (A^{(2)}_{F'm,f'\mu} + \Omega_1^{f',F'} A^{(1)}_{F'm,f'\mu}) = i\lambda_{Fm,f\mu} \delta\rho_{Fm,f\mu} + \sum_{F',f'} (\Omega_1^{f',F'})^2 \Lambda(\delta\rho)_{F'm,f'\mu}, \quad (17)$$

where the elements $A^{(2)}_{Fm,f\mu}$, $A^{(1)}_{Fm,f\mu}$, $\lambda_{Fm,f\mu}$, and $\Lambda(\delta\rho)_{Fm,f\mu}$ are defined in the Appendix. TBS signals calculated along these lines for all components of the Na D_1 line are shown in Figs. 7(a)–Fig. 7(d). As in the SBS case, they are symmetric around $\omega_B=0$ [the insets in Fig. 7(b) and Fig. 7(d) show expanded details of the TBS signals around zero field].

An important advantage of the TBS is the possibility of selection of a given hfs component from a complex transition whose Doppler width exceeds the hyperfine splitting. For single transitions where no such selection is necessary the TBS and SBS signals should be similar. This is indeed the case, as can be seen by comparison of the signals represented by the lines with dots in Fig. 7 with the signals in Figs. 2–5. On the other hand, for the case of complex transitions the

TBS and SBS signals differ dramatically. In Fig. 7 the solid lines without dots, labeled D_1, represent the TBS signals calculated for Doppler-free selection of various hfs components by appropriate laser tuning with all remaining, nonresonant components of the complex transitions also taken into account. The most significant difference between the TBS signals calculated for complex and single transitions is the presence of additional, very narrow structure close to $\omega_B=0$ seen when ω_L is tuned to any hfs component of the Na D_1 line except $F=2\leftrightarrow f=1$. The structure is much narrower than the signals for single transitions (lines with dots in Fig. 7) and the SBS signals (Figs. 2–5). One could expect that, because of their small width, these structures would be associated with the highest possible multipole rank. In such a case, however, these narrow structures should be seen also in the signals obtained for isolated transitions, which is not the case.

As can be seen by comparison of the solid and broken curves in Fig. 7(b), there is clear evidence of the hexadecapole contribution in the case of the $F=2\leftrightarrow f=2$ transition. However, in contrast to the SBS signals (Fig. 2), the hexadecapole contribution is not the narrowest feature of the TBS signals. This is caused by a substantial power broadening of the hexadecapole resonance which, for the cases illustrated in Fig. 7(b), peaks around $\omega_B=3$ MHz. The narrow structure shown by the solid line is due to the contributions of the nonresonant hfs components of the complex line and not to the hexadecapole in the Doppler-free-selected hfs component. To understand the origin of this narrow feature of the signals for complex lines seen in [Figs. 7(a)– 7(c)] around $\omega_B=0$ we have to analyze solutions of Eq. (16) [given in the Appendix by (A2)–(A4)] in more detail. To first order in E_2 these solutions [Eq. (A4)] consist of two distinct contributions: $A^{(2)}_{F'm',f'\mu'}$ which depend on Zeeman coherences and populations, and $A^{(1)}_{F'm',f'\mu'}$ which are related with optical coherences $\rho_{f\mu,Fm}$. The $A^{(2)}_{F'm',f'\mu'}$ terms enter the solutions (A4) multiplied by $\Omega_2^{f',F'}$, whereas the $A^{(1)}_{F'm',f'\mu'}$ terms are multiplied by $\Omega_1^{f',F'}\Omega_2^{f',F'}$. Since $\Omega_1^{f',F'}\gg\Omega_2^{f',F'}$, the TBS signals are dominated by the $A^{(1)}_{F'm',f'\mu'}$ contributions and are given by the following, approximate relation:

$$I_{\mathrm{TBS}}(\mathbf{r}_0)\approx N^2\sum_{m',\mu'}\alpha^{m',\mu'}_{m,\mu}|\Omega_1^{f,F}A^{(1)}_{F'm',f'\mu'}|^2, \qquad (18)$$

where coefficients $\alpha^{m',\mu'}_{m,\mu}$ depend on $T^{F'm',f'\mu'}_{Fm,f\mu}$ introduced in (A4), on $\Omega_2^{f,F}$, and depends on transition-matrix elements. For a complex transition Eq. (A2) for $A^{(1)}_{F'm',f'\mu'}$ involves all hfs components, including the nonresonant ones. Thus, even when a given $F\leftrightarrow f$ transition is Doppler-free selected by a proper tuning of ω_L the contributions like

$$\sum_{F'\neq F}\sum_{m',\mu'}\frac{1}{\lambda_{f\mu',f\mu}}D^{F,f}_{m,\mu'}\rho_{f\mu',F'm'}D^{F',f}_{m',\mu}\times(\delta_{m',\mu-1}-\delta_{m',\mu+1}) \qquad (19)$$

(and similarly with denominator $\lambda_{Fm,Fm'}$) cannot be neglected in $A^{(1)}_{F'm',f'\mu'}$. It is important that even when the amplitude of the $\rho_{f\mu,F'm'}$ elements is small because of a nonresonant $F'\leftrightarrow f$ excitation, terms (19) can be relevant close to $\omega_B=0$ due to resonant enhancement by the $\lambda^{-1}_{f\mu',f\mu}$ factors. Obviously, such an enhancement at $\omega_B\approx0$ takes place also for resonant components but in that case the $\rho_{f\mu,F'm'}(\omega_B)$ dependence becomes saturated and strongly power broadened. For these reasons in weak magnetic fields ($\omega_B\approx0$) the TBS signals associated with complex transitions are mainly affected by nonsaturated optical coherences on nonresonant components, while for higher ω_B the TBS signals are due to coherences on the components resonantly selected by the probe beam. The TBS method eliminates the need for velocity averaging but does not allow one to neglect the nonresonant hfs components which add their narrow, not power-broadened contributions to the net scattered intensity. It is interesting that these narrow, nonresonant contributions do not occur for the SBS case. It is related to a perfect phase matching (coherence) of individual atomic contributions to the scattered light. Some of these contributions are of opposite sign to those given by (19) which results in their exact cancellation. In the TBS case many terms average to zero after position integration and such cancellation is not perfect, leaving nonzero terms (19).

The narrow structures arising from nonresonant contributions to TBS are very sensitive to the relaxation rates of the Zeeman coherences and populations appearing in denominators $\lambda_{f\mu',f\mu}$, as well as to the relaxation rates of the optical coherences $\rho_{f\mu,F'm'}$. For illustration of the dependence of the TBS signals on collisional relaxation we show in Fig. 8 a series of the TBS signals calculated for Doppler-free selection of various hfs components in the Na D_1 line and for various collisional relaxation rates. For the sake of simplicity, we have assumed that the collisions affect the coherences in the lower and upper states in the same way: $\gamma_e^{m,m'\neq m}=\gamma_e+\Gamma$, $\gamma_g^{\mu,\mu'\neq\mu}=\gamma_g+\Gamma$, and $\gamma=(\gamma_g+\gamma_e)/2+\Gamma$, where Γ is the collisional relaxation rate. Figure 8 shows a very strong dependence of the TBS signals on Γ for all hfs components. When $\Gamma>2\pi\times1$ MHz the narrow structures attributed above to the nonresonant components (narrow maxima around $\omega_B=0$) disappear and the signals decrease monotonically with Γ. In the range of $\Gamma\leqslant2\pi\times1$ MHz, the TBS signals depend very sensitively on changes of Γ as small as $2\pi\times10$ kHz. Such a strong dependence suggests application of the TBS for studies of collisions, particularly in the cases of low pressure or low cross section.

IV. ROLE OF THE TRAP STATES

Standard interpretation of FS signals is based on analysis of the evolution of Zeeman and optical coherences in a magnetic field. Due to mutual couplings between all elements of the density matrix, Zeeman coherences associated with a given multipole order can be detected by changes of the optical coherences which, according to Eqs. (9) and (16), determine the FS signals. It is important that even with a weak probe beam these couplings between density-matrix elements allow detection of contributions arising from Zeeman coherences with $\Delta m>2$, i.e., from multipole moments of higher than quadrupole rank.

The standard interpretation explains resonant changes of the forward-scattered light around $\omega_B=0$ in a similar way to

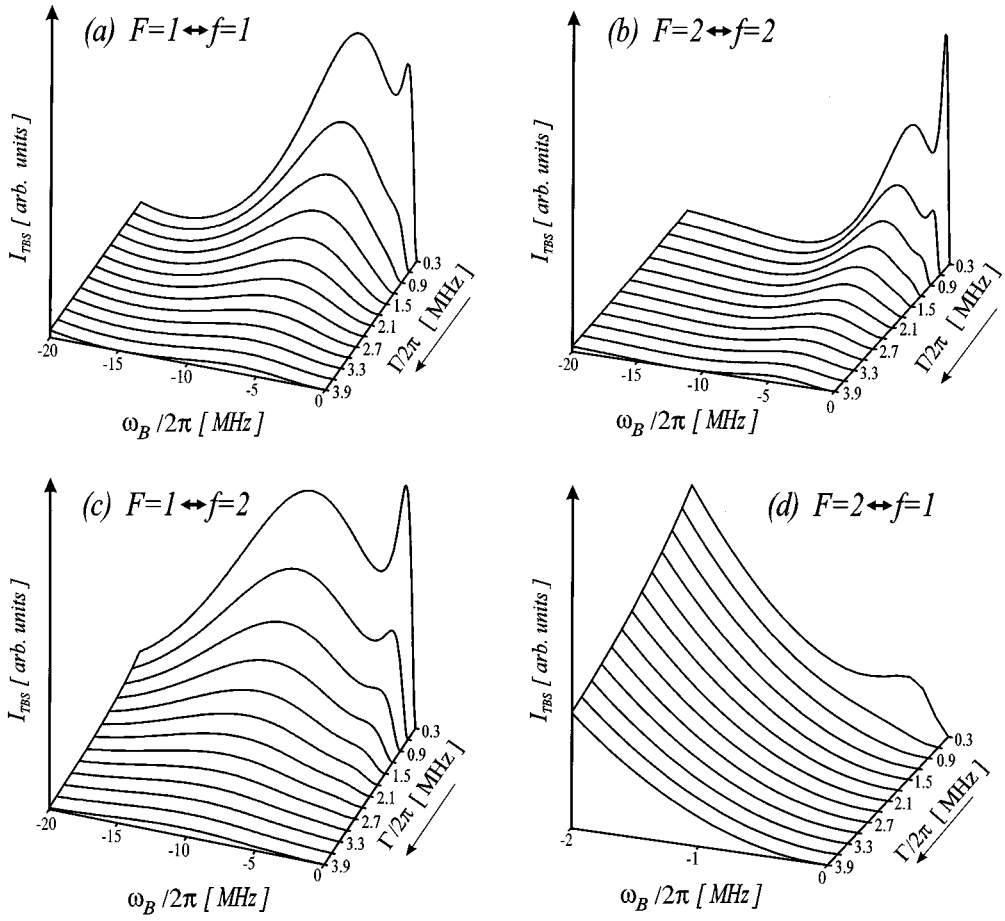

FIG. 8. The TBS spectra for various Na D_1 components versus relaxation rate Γ and for $\Omega_0=2\pi\times 45$ MHz. For simplicity, in these simulations we do not distinguish between relaxation rates of the Zeeman coherences related to hexadecapole and quadrupole multipoles. The relaxation rates of optical coherences are $\gamma=(\gamma_e+\gamma_g)/2+\Gamma$.

the Hanle effect in fluorescence, i.e., as destruction of the light-induced Zeeman coherences by the Larmor precession (magnetic mixing) [5]. The frequency of this precession (or the magnetic mixing rate) equals $g\mu_B\Delta mB$. The coherences are maximal when $B=0$ (zero-field level crossing) and the magnitude of the precession frequency, or the intensity of the magnetic field, necessary for coherence destruction depends on relaxation rates (width of the crossing levels). As pointed out in Sec. III A, since the precession frequency is proportional to Δm it should be feasible to distinguish the contributions of various coherences (multipoles) owing to various widths of their resonances in I_{FS}. When $\omega_B\neq 0$, the $\sigma^{\pm}$ components of light transmitted are phase shifted in opposite senses, which causes rotation of the polarization plane (nonlinear Faraday effect) and nonzero signal $I_{\mathrm{FS}}(B\neq 0)\neq 0$.

Such an approach allows correct calculation of FS signals but is not very physically comprehensive, particularly in the nonperturbative regime. For instance, it does not explain such signal features as the striking difference between the hexadecapole contributions to the $F=2\leftrightarrow f=2$ and $F=1\leftrightarrow f=2$ transitions demonstrated above in Sec. III. Below, we shall present the interpretation of FS in terms of trap states that allows relating FS signals to such fundamental characteristics as the symmetry of given atomic transitions correlated with a number of possible states and with their evolution in a magnetic field. This not only simplifies interpretation of the FS signals but also allows studies of the role of trap states in atomic systems of higher angular momenta.

Depending on the particular configuration of the system under consideration, and specifically on whether $F>f$, $F=f$, or $F<f$, there are, respectively, 0, 2, or 1 stable traps in the ground state [17]. We are here interested mainly in the ground-state traps as they are not destroyed by spontaneous emission and are ideal traps for $B=0$. In the excited states stable traps can be created only when the Rabi frequency is sufficiently big with respect to the spontaneous emission rate. Having defined the appropriate basis of coupled and trap states we can use it for representation of all relevant operators and their expectation values such as, e.g., the Hamiltonian and the intensity of the forward-scattered light. This intensity depends on optical coherences between trap and coupled states. Such coherences are zero when the traps are perfect, i.e., when $B=0$, hence $I_{\mathrm{FS}}(B=0)=0$. Nonzero intensity of the forward-scattered light is due to imperfections of the traps resulting from transitions (e.g., magnetic-field induced) between coupled and uncoupled states.

The properties and form of the forward-scattering signals can thus be related to the dynamics of the coupling of the

trap and coupled states. For specific angular momenta trap states can be associated with superpositions of various magnetic sublevels, i.e., with given Zeeman coherences and multipole moments. When symmetry of the transition allows existence of two trap states, an external magnetic field couples them and causes their competition. It is due to this competition that FS signals can be dominated by the quadrupole trap, even in systems where generation of the hexadecapole traps is possible. Below, we discuss such effects in a detailed way for each of the above analyzed transitions (except of the $F=2\leftrightarrow f=1$ one, which has trap states similar to $F=1\leftrightarrow f=2$ but unstable with respect to spontaneous emission) .

A. Transition $F=1\leftrightarrow f=1$

Neglecting spontaneous emission, we can define the new basis for the $F=1\leftrightarrow f=1$ transition in a standard way as composed of coupled and uncoupled states [16,17],

$$|t\rangle=\frac{1}{\sqrt{2}}(|f,-1\rangle+|f,+1\rangle) \quad \text{(uncoupled-trap state)}, \tag{20}$$

$$|s\rangle=\frac{1}{\sqrt{2}}(|f,-1\rangle-|f,+1\rangle) \quad \text{(coupled state)}, \tag{21}$$

$$|f,0\rangle \quad \text{(coupled state)} \tag{22}$$

for the lower state and analogously with states $|T\rangle$, $|S\rangle$, and $|F,0\rangle$ for the upper state.

States $|t\rangle$ and $|T\rangle$ are traps, while $|s\rangle$ and $|S\rangle$ are coupled states. However, with spontaneous emission taken into account, the upper state becomes unstable and so does superposition $|T\rangle$. State $|t\rangle$ associated with the ground state remains then as the only stable trap. Superpositions defined by (20)–(22) are associated with Zeeman coherences of the $\rho_{-1,+1}$ kind, i.e., with the quadrupole moments in $f=1$ and $F=1$.

In the new basis atomic and interaction parts of the Hamiltonian are

$$H_{1,1}^{F,f}=-g_{f=1}\omega_B(|t\rangle\langle s|-|s\rangle\langle t|)-g_{F=1}\omega_B(|T\rangle\langle S|-|S\rangle\langle T|) + \left[i\Omega_0\sqrt{\frac{1}{12}}(|s\rangle\langle F,0|-|f,0\rangle\langle S|)+\text{H.c.}\right]. \tag{23}$$

Using Eq. (9) and transformation (20)–(22) the intensity of the forward-scattered light in our geometry with crossed polarizers can be expressed as

$$I_{\text{SBS}}\propto N^2|\langle|F,0\rangle\langle t|-|T\rangle\langle f,0|\rangle|^2 . \tag{24}$$

Equation (24) relates the forward-scattering signals to mixing between trap superpositions $|t\rangle$, $|T\rangle$ and coupled sublevels $|F,0\rangle$, $|f,0\rangle$. As long as the traps are perfect, i.e., as long as $\omega_B=0$ and there is no magnetic coupling between $|t\rangle$ and $|s\rangle$ ($|T\rangle$ and $|S\rangle$) represented by the first two terms in (23), no such mixing is possible and $I_{\text{SBS}}=0$. We have here a full analogy between the scattering signals and the coherent-population trapping [16]. For $\omega_B\neq 0$, however, the structure of the forward-scattering signal $[I_{\text{SBS}}(B)]$ will be determined by magnetic precession of the quadrupolar coherences in both lower and upper levels, i.e., the $|s\rangle$-$|t\rangle$ ($|S\rangle$-$|T\rangle$) magnetic mixing. States $|t\rangle$, $|T\rangle$ remain efficient traps for such ω_B which allow existence of these coherences but lose their trapping characteristics when the precession becomes faster than appropriate relaxation rates. When the lower state is a long-lived ground state, the width of a resulting FS resonance around $\omega_B=0$ will be mainly determined by the atomic transit time and power broadening (Fig. 5). Because the upper-state trap $|T\rangle$ is quenched by spontaneous emission, the contribution of the upper-state quadrupole can be seen only when the light beam is sufficiently strong that Ω_0 is comparable to the spontaneous emission rate. When the lower- and upper-state relaxation rates are sufficiently different, the FS signals exhibit a clear double structure arising from the quadrupole moments induced in both states. For the range of ω_B used for Fig. 5 the excited-state contribution is not apparent.

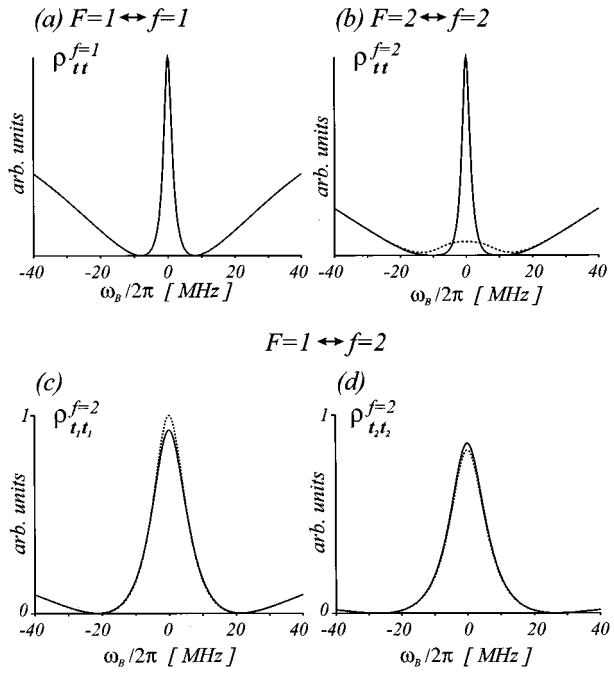

FIG. 9. Calculated populations of trap states for different single transitions versus Larmor frequency ω_B. (c) and (d) are plotted in the same scale. Solid and dotted lines represent the populations calculated with and without hexadecapole moments, respectively. Resonant excitation with $\Omega_0=2\pi\times 25$ MHz is assumed.

To illustrate the analogy between FS signals and CPT it is interesting to compare the $I_{\text{SBS}}(\omega_B)$ signal with the magnetic-field dependence of the population of the trap state $\rho_{tt}^{f=1}=\text{Tr}\{|t\rangle\langle t|\}$. Such a dependence, calculated for resonant excitation, is shown in Fig. 9(a), which illustrates a very strong increase of the $\rho_{tt}^{f=1}$ populations around $\omega_B=0$. Comparing Figs. 5 and 9(a) we see that the $\rho_{tt}^{f=1}(\omega_B)$ dependence resembles an inverted FS signal and the ranges of efficient population trapping correspond well to the range of strong variation of I_{SBS}.

B. Transition $F=2\leftrightarrow f=2$

The new basis is taken in the form

$$|t\rangle=\frac{1}{2}\sqrt{\frac{3}{2}}\left(|f,-2\rangle+|f,+2\rangle+\sqrt{\frac{2}{3}}|f,0\rangle\right) \quad \text{(trap state)}, \tag{25}$$

$$|s_1\rangle=\sqrt{\frac{1}{2}}(|f,-2\rangle-|f,+2\rangle) \quad \text{(coupled state)}, \tag{26}$$

$$|s_2\rangle=\sqrt{\frac{1}{8}}(|f,-2\rangle+|f,+2\rangle-\sqrt{6}|f,0\rangle) \quad \text{(coupled state)}, \tag{27}$$

$$|s_3\rangle=\sqrt{\frac{1}{2}}(|f,-1\rangle-|f,+1\rangle) \quad \text{(coupled state)}, \tag{28}$$

$$|s_4\rangle=\sqrt{\frac{1}{2}}(|f,-1\rangle+|f,+1\rangle) \quad \text{(coupled state)} \tag{29}$$

for the lower state $f=2$ and analogously for the upper state $F=2$ where capital letters T, S, F replace t, s, f to distinguish between the two sets of states. In (25)–(29) states $|t\rangle$, $|T\rangle$ are trap states that are related to the hexadecapole coherences. The atomic and interaction parts of the Hamiltonian transformed to the above representation are

$$\begin{aligned}H_{2,2}^{F,f}=&-g_{f=2}\omega_B(\sqrt{3}|t\rangle\langle s_1|+|s_1\rangle\langle s_2|+|s_3\rangle\langle s_4|+\text{H.c.})\\&-g_{F=2}\omega_B(\sqrt{3}|T\rangle\langle S_1|+|S_1\rangle\langle S_2|+|S_3\rangle\langle S_4|+\text{H.c.})\\&-\left[i\Omega_0\left[\sqrt{\frac{1}{3}}(|s_3\rangle\langle S_2|-|s_2\rangle\langle S_3|)\right.\right.\\&\left.\left.-\sqrt{\frac{1}{12}}(|s_1\rangle\langle S_4|-|s_4\rangle\langle S_1|)\right]+\text{H.c.}\right].\end{aligned} \tag{30}$$

$H_{2,2}^{F,f}$ has a very similar structure to $H_{1,1}^{F,f}$ in that it consists of terms representing magnetic mixing between trap $|t\rangle$ ($|T\rangle$) with $|s_1\rangle$ ($|S_1\rangle$) and between other coupled states or a coherent coupling of coupled superpositions in the lower state with coupled superpositions in the upper state. Similarly, the intensity of forward-scattered light can be expressed as the result of mixing between various states:

$$\begin{aligned}I_{\text{SBS}}\propto N^2\left|\left\langle\frac{1}{2}(|S_4\rangle\langle t|+|T\rangle\langle s_4|)-\sqrt{\frac{1}{3}}(|S_4\rangle\langle s_2|+|S_2\rangle\langle s_4|)\right.\right.\\\left.\left.+\sqrt{\frac{1}{12}}(|S_1\rangle\langle s_3|+|S_3\rangle\langle s_1|)\right\rangle\right|^2.\end{aligned} \tag{31}$$

For $\omega_B\approx 0$ the relevant term of expression (31) is the first one, proportional to the trap state in ground $f=2$ level. For nearly zero magnetic field, the traps $|t\rangle$ and $|T\rangle$ are nearly perfect, yet $|T\rangle$ is unstable because of spontaneous emission. Spontaneous emission results in decay of $|T\rangle$ and in zero population of all coupled states, so, similarly as for the $F=1\leftrightarrow f=1$ transition it is only state $|t\rangle$ whose dynamics is decisive for properties of the scattering signal. This time, however, $|t\rangle$ is associated with the hexadecapole moment (superposition of $|f,\pm 2\rangle$ and $|f,0\rangle$), so the corresponding resonance around $\omega_B=0$ is narrower (nearly by a factor 2 if power broadening could be ignored) than in the case of the $F=1\leftrightarrow f=1$ transition. The analogy between the scattering signal and coherent-population trapping is seen, by comparison of Fig. 9(b) where we plot population of the trap $\rho_{tt}^{f=2}$ for $f=2$ versus ω_B with the $I_{\text{SBS}}(\omega_B)$ dependence in Fig. 2. As for the $F=1\leftrightarrow f=1$ case the magnetic dependence of $\rho_{tt}^{f=2}$ resembles the inverted FS signal. Moreover, both dependencies are dramatically sensitive on the hexadecapole coherence: its elimination yields CPT and scattering resonances [depicted in Figs. 9(b) and 2 by dashed lines] much broader and weaker than when they are properly accounted for (solid lines).

C. Transition $F=1\leftrightarrow f=2$

For this transition the elements of the new basis are

$$|t_1\rangle=\sqrt{\frac{1}{2}}(|f,-1\rangle-|f,+1\rangle) \quad \text{(trap state)}, \tag{32}$$

$$|t_2\rangle=\sqrt{\frac{1}{8}}(|f,-2\rangle+|f,+2\rangle-\sqrt{6}|f,0\rangle) \quad \text{(trap state)}, \tag{33}$$

$$|s_1\rangle=\sqrt{\frac{1}{2}}(|f,-1\rangle+|f,+1\rangle) \quad \text{(coupled state)}, \tag{34}$$

$$|s_2\rangle=\sqrt{\frac{1}{2}}(|f,-2\rangle-|f,+2\rangle) \quad \text{(coupled state)}, \tag{35}$$

$$|s_3\rangle=\frac{1}{2}\sqrt{\frac{3}{2}}\left(|f,-2\rangle+|f,+2\rangle+\sqrt{\frac{2}{3}}|f,0\rangle\right) \text{(coupled state)} \tag{36}$$

for the lower state $f=2$ and

$$|S_1\rangle=\sqrt{\frac{1}{2}}(|F,-1\rangle+|F,+1\rangle) \quad \text{(coupled state)}, \tag{37}$$

$$|S_2\rangle=\sqrt{\frac{1}{2}}(|F,-1\rangle-|F,+1\rangle) \quad \text{(coupled state)}, \tag{38}$$

$$|F,0\rangle \quad \text{(coupled state)} \tag{39}$$

for the upper state $F=1$. With transformation (32)–(39) the atomic and interaction part of the Hamiltonian is

$$\begin{aligned}H_{1,2}^{F,f}=&-g_{f=2}\omega_B[\sqrt{3}|s_2\rangle\langle s_3|+|s_2\rangle\langle t_2|+|t_1\rangle\langle s_1|+\text{H.c.}]\\&-g_{F=1}\omega_B(|S_1\rangle\langle S_2|+\text{H.c.})-\left[i\Omega_0\left(\sqrt{\frac{1}{3}}|s_3\rangle\langle S_1|\right.\right.\\&\left.\left.+\frac{1}{2}(|s_2\rangle\langle S_2|+|s_1\rangle\langle F,0|)\right)+\text{H.c.}\right].\end{aligned} \tag{40}$$

Similarly as in the previous cases we express the forward-scattered light intensity in terms of the new states (32)–(39) which yields

$$I_{\mathrm{SBS}} \propto N^2 \left| \left\langle |S_1\rangle\langle s_2| + |F,0\rangle\langle t_1| + \sqrt{\frac{1}{3}}|S_2\rangle\left(\sqrt{3}\langle t_2| + \langle s_3|\right)\right\rangle \right|^2 . \tag{41}$$

In the region of small magnetic fields, most interesting for the FS signals, the traps are nearly perfect and accumulate most of the atomic populations. Equation (41) can then be approximated to yield

$$I_{\mathrm{SBS}} \propto N^2 |\langle |F,0\rangle\langle t_1| + |S_2\rangle\langle t_2|\rangle|^2 . \tag{42}$$

As we see from Eq. (42), for $\omega_B \approx 0$, the scattering signal is determined by contributions of both trap states existing for the $F=1 \leftrightarrow f=2$ transition. Since traps $|t_1\rangle$ and $|t_2\rangle$ are related to different ground-state sublevels and different multipole moments, it would be natural to expect contributions of different (quadrupole and hexadecapole) multipoles to the scattering signals. However, as seen in Fig. 3, the forward-scattering signals for the $F=1 \leftrightarrow f=2$ transition have only one resonant contribution around $\omega_B=0$, not much different from the signals characteristic for the $F=1 \leftrightarrow f=1$ transition dominated by a single, quadrupole trap (Fig. 3).

This unexpected insensitivity of the $F=1 \leftrightarrow f=2$ transitions on the hexadecapole coherence is caused by the existence of two subsystems containing $|t_1\rangle$ and $|t_2\rangle$ and their coupling by spontaneous emission. As we see from (40), there are two sets of states $\{|t_2\rangle,|s_2\rangle,|s_3\rangle,|S_1\rangle,|S_2\rangle\}$, and $\{|t_1\rangle,|s_1\rangle,|F,0\rangle\}$, coupled within each set by the magnetic and laser fields, each of them involving one of the traps. The two sets are independent when $\omega_B=0$ and Hamiltonian (40) represents the only relevant interaction. When $\omega_B \neq 0$, $|t_1\rangle$ and $|t_2\rangle$ are mixed with coupled states and their populations, after subsequent excitation, are again redistributed by spontaneous emission, among trap and coupled states of both sets. Such redistribution leads to equalization of population of $|t_1\rangle$ and $|t_2\rangle$ which can be seen in Figs. 9(c) and 9(d) where we have depicted magnetic-field dependencies of $\rho^{f=2}_{t_1t_1}$ and $\rho^{f=2}_{t_2t_2}$ with (solid lines) and without (dashed lines) hexadecapole coherences. The fact that populations of $|t_1\rangle$ and $|t_2\rangle$ depend very little on the hexadecapole moment corresponds to the very weak dependence of the scattering signals for the $F=1 \leftrightarrow f=2$ transition on the hexadecapole (Fig. 3) discussed above. As seen from Figs. 9(c) and 9(d) not only the amplitudes but also the width of the population dependencies on ω_B are similar for $|t_1\rangle$ and $|t_2\rangle$. This might seem to be inconsistent with the expectation to see hexadecapole resonances around zero magnetic field about two times narrower than the quadrupole ones. However, due to the coupling between the subsystems involving $|t_1\rangle$ and $|t_2\rangle$ by spontaneous emission, populations are equalized between these two traps for any nonzero value of ω_B, which is responsible for nearly equal width of the curves in Figs. 9(c) and 9(d).

The mixing between $|t_1\rangle$ and $|t_2\rangle$ explains also a small difference in the width of solid and broken curves seen in Fig. 3. Though the difference is rather small it is interesting that the signals with the hexadecapole coherences are slightly broader than those without the hexadecapole, with only the quadrupole coherence. This is due to the fact that when the hexadecapole is not quenched trap $|t_2\rangle$ is efficient and not much of its population is transferred to $|t_1\rangle$. On the other hand, without the hexadecapole coherence population of $|t_1\rangle$ increases, so the FS signals are narrower without than with the hexadecapole. Thus, for the $F=1 \leftrightarrow f=2$ transition, where no direct signature of the hexadecapole moment in the FS signals is seen, it is the indirect effect of this multipole on the signal width that can be used as its possible evidence.

D. The complex transition with hfs-Na D_1 line

Again we focus here on the D_1 component of the sodium fine structure doublet. For a complex transition contributions of all individual hfs components must obviously be accounted for. This becomes a very simple addition of independent contributions, analyzed above, with appropriate weights determined by laser frequency and atomic velocity distribution for the case when the hfs is well resolved with respect to the Doppler width. In the opposite case the individual hfs components cannot be considered individually, because of their mutual coupling by nonresonant laser excitation and spontaneous emission.

For the Na D_1 transition the decisive contributions to the scattering signal come from only two hfs components which are associated with the $f=2$ ground-state sublevel: $F=1,2 \leftrightarrow f=2$. Two components with $f=1$ are at least one order of magnitude weaker and can be neglected in a qualitative analysis. The two relevant components share the same lower level where, in principle, the quadrupole as well as hexadecapole coherences can be induced by the σ-polarized laser light. We have shown above that the FS signals associated with the $F=2 \leftrightarrow f=2$ component exhibit very clear hexadecapole resonance whereas those related with the $F=1 \leftrightarrow f=2$ component are dominated by the quadrupole moment. The two components differ only in their upper levels which are split by only 189 MHz, which is much less than the Doppler width of about 1 GHz for typical experimental conditions. Thus for any laser frequency within the Doppler profile of the D_1 transition both components are excited with comparable efficiency. Simple addition of the contributions of these two components (we recall that the nonresonant components are taken into account when calculating elements of ρ) should then yield scattering signals containing signatures of the quadrupole and hexadecapole moments around $\omega_B=0$. However, as was shown in Fig. 6, the FS signal calculated for the whole D_1 transition is dominated by the quadrupole moment only, the $F=2 \leftrightarrow f=2$ component with its hexadecapole contribution constitutes only about 10% of the total signal.

Explanation of this surprising fact is based on the coupling by spontaneous emission between the $|t_1\rangle$ and $|t_2\rangle$ traps found in the $F=1 \leftrightarrow f=2$ dynamics which destroys any possible hexadecapole contribution to $|t_2\rangle$. Additionally, as seen by comparison of Eqs. (25) and (36), the superposition which represents trap state $|t\rangle$ for $F=2 \leftrightarrow f=2$ transition is almost equal to coupled state $|s_3\rangle$ for the $F=1 \leftrightarrow f=2$ transition, and vice versa, the states which are traps for the $F=1 \leftrightarrow f=2$ component ($|t_1\rangle$, $|t_2\rangle$) became coupled states

($|s_3\rangle$, $|s_2\rangle$) for $F=2\leftrightarrow f=2$. When both components are excited with comparable efficiency, the above coupling between trap and coupled states results in domination of the total scattering signal by the lowest-order coherences, i.e., quadrupole moments. The higher-order coherences, like the hexadecapole in our example, do not survive such competition, which explains why the D_1 signals are associated mainly with the quadrupole moment.

V. CONCLUSIONS

We have performed nonperturbative analysis of the role of multipole moments in the forward scattering of resonance light on atoms in a magnetic field. Its results solved the long-lasting controversy around the observability of the hexadecapole moment in FS on sodium atoms. By simulating the FS signals on single transitions between levels with angular momenta 1 and 2 we have shown that, unlike fluorescence experiments, the FS signals on the $F=1\leftrightarrow f=2$ transition very weakly depend on the hexadecapole moment whereas the $F=2\leftrightarrow f=2$ one is very strongly affected by this multipole. When the laser is tuned to the Na D_1 line with its unresolved hfs components the FS signals are dominated by the contributions of the $F=1\leftrightarrow f=2$ component which has almost no hexadecapole signature. This explains why no evidence of the hexadecapole moment was found in the recent experiment of Holmes and Griffith [15] and proves that also in the early experiment of Gawlik *et al.* [6] there was no hexadecapole contribution to the D_1 signals. This clearly shows that there is very little influence of the hexadecapole moment in the FS experiments with a single light beam tuned to the Na D_1 line [6]. Another interesting finding is that the $F=2\leftrightarrow f=2$ signals which are significantly affected by the hexadecapole are very similar to those for the $F=1\leftrightarrow f=1$ component where the quadrupoles are the highest-rank multipoles. This conclusion, however, does not justify using the perturbative approach for analysis of the FS signals with strong laser light. Comparison of the signals calculated for single $F=2\leftrightarrow f=2$ transitions with its strong hexadecapole signature with the $F=1\leftrightarrow f=1$ one where quadrupoles are the highest-rank multipoles indicates that the simple lineshape similarity could be very misleading. For this reason it is very unlikely that the FS experiments of Ståhlberg *et al.* [13] with well resolved neon transition $F=2\leftrightarrow f=2$ could be properly interpreted within the third-order perturbation theory involving only quadrupole moments.

In addition to the single-beam scattering we have also analyzed the pump-probe TBS method which allows Doppler-free selection of a given hfs component of a complex line. The TBS simulations revealed narrow structure of the FS signals around zero magnetic field which, contrary to the intuitive expectations, is not related to the highest-order multipole but is rather due to the nonresonant hfs components. These narrow structures are very sensitive to collisions which could find practical spectroscopic applications.

We have interpreted the calculated results in terms of the trap states. We showed that the number and mutual couplings between various traps and between traps and coupled states determine the character of the FS signals. Symmetry of a transition is directly related to the number of traps and allows determination of the scattering signals.

ACKNOWLEDGMENTS

We are very grateful to Dr. Jerzy Zachorowski for numerous detailed discussions. This work was supported by the EU (Grant No. COST CIPA-CT93-0094) and by the Polish Committee of Scientific Research KBN (Grant No. 2PO3B113-10).

APPENDIX

As seen from Eq. (16), calculation of the TBS signals requires finding the $\delta\rho_{Fm,f\mu}$ elements. Equations for these collective variables are obtained from Eqs. (2)–(7) in the steady-state limit with several approximations. In particular, except for studies of collisional effects (Fig. 8) we consider the case of radiative relaxation and neglect (i) all elements with the atomic position dependence, e.g., $\Sigma_l \rho_{Fm,f\mu} e^{\pm i(\mathbf{k}_1-\mathbf{k}_2)\cdot\mathbf{r}_l}$; (ii) couplings with $\Sigma_l \delta\rho_{f\mu,Fm} e^{-i(2\mathbf{k}_1-\mathbf{k}_2)\cdot\mathbf{r}_l}$, i.e., couplings with four-wave-mixing contributions; and (iii) couplings of the $\delta\rho_{Fm,f\mu}$ elements for the $F\leftrightarrow f$ transition with elements $\delta\rho_{F'm',f'\mu'}$ belonging to different transitions ($F\neq F'$ and $f\neq f'$). The $\delta\rho_{F'm',f'\mu'}$ elements introduce the $\sim 1/(i\gamma+\Delta_{F',f'})$ weight factors into the equations ($\sim\Delta_{F',f'}=\omega_0^{F'}-\omega_0^{f'}-\omega_L$) which are negligible for big detunings (hfs splittings). Neglecting (i) is justified by destructive interference in integration over atomic positions, while the contributions mentioned in (ii) represent higher-order processes, of a smaller amplitude.

By expanding the single-atom density matrix to first order in the E_2 field [Eq. (13)] and using the steady-state approximation, algebraic equations for the $\delta\rho^{(l)}_{Fm,f\mu}$ corrections to optical coherences can be obtained after straightforward, yet tedious, algebra. After position averaging, Eq. (17) is obtained for the averaged, collective quantities $\delta\rho_{Fm,f\mu}=\Sigma_l \delta\rho^{(l)}_{Fm,f\mu}$ The coefficients appearing in (17) are defined below by Eqs. (A1)–(A3).

$$\begin{aligned}\Lambda(\delta\rho)_{Fm,f\mu} = i\sum_{f'\mu'}\sum_{F'm'}\Bigg(&\frac{1}{\lambda_{f'\mu',f\mu}} D^{F,f'}_{m,\mu'} D^{f',F'}_{\mu',m'}\delta\rho_{F'm',f\mu} \\ &+ \frac{1}{\lambda_{Fm,F'm'}}\delta\rho_{Fm,f'\mu'} D^{F',f'}_{\mu',m'} D^{F',f}_{m',\mu}\Bigg) \\ &+ 2\gamma_e \sum_{f'\mu'}\sum_{f''\mu''}\frac{1}{\lambda_{f'\mu',f\mu}} D^{F,f'}_{m,\mu'} \\ &\times\sum_{F'm'}\sum_{F''m''}\frac{1}{\lambda_{F'm',F''m''}} \\ &\times D^{f',F'}_{\mu',m'}\delta\rho_{F'm',f''\mu''} D^{f'',F''}_{\mu'',m''} D^{F'',f}_{m'',\mu}, \qquad \text{(A1)}\end{aligned}$$

$\lambda_{Fm,F'm'}=i\gamma_e^{m,m'}-(m-m')\omega_B$, $\lambda_{f\mu,f'\mu'}=i\gamma_g^{\mu,\mu'}-(\mu-\mu')\omega_B$, where $\gamma_e^{m,m'}$ and $\gamma_g^{\mu,\mu'}$ are relaxation rates of matrix elements $\rho_{Fm,Fm'}$ and $\rho_{f\mu,f\mu'}$ with respect to collisions, respectively.

$$\lambda_{Fm,f\mu}=-i\gamma-\Delta_{F,f}-(mg_F-\mu g_f)\omega_B$$

and

$$\gamma=\frac{(\gamma_e+\gamma_g)}{2}, \quad \Delta_{F,f}=\omega_F-\omega_f-\omega_L,$$

$$A^{(1)}_{Fm,f\mu}=i\Bigg[\sum_{F'}\sum_{m',\mu'}\frac{1}{\lambda_{f\mu',f\mu}}D^{F,f}_{m,\mu'}\rho_{f\mu',F'm'}D^{F',f}_{m',\mu}\times(\delta_{m',\mu-1}-\delta_{m',\mu+1})-\sum_{f'}\sum_{m',\mu'}\frac{1}{\lambda_{Fm,Fm'}}D^{F,f'}_{m,\mu'}\rho_{f'\mu',Fm'}D^{F,f}_{m',\mu}\times(\delta_{\mu',m-1}-\delta_{\mu',m-1})\Bigg]-2\gamma_e\sum_{f''}\sum_{\mu',\mu''}\frac{1}{\lambda_{f\mu',f\mu}}D^{F,f}_{m,\mu'}\sum_{F'}\sum_{m',m''}\times\frac{1}{\lambda_{F'm',F'm''}}D^{f,F'}_{\mu',m'}D^{F',f''}_{m',\mu''}\rho_{f''\mu'',F'm''}D^{F',f}_{m'',\mu}\times(\delta_{\mu'',m'-1}-\delta_{\mu'',m'+1}),\tag{A2}$$

$$A^{(2)}_{Fm,f\mu}=\sum_{\mu'}D^{F,f}_{m,\mu'}\rho_{f\mu',f\mu}(\delta_{\mu',m-1}-\delta_{\mu',m+1})+\sum_{m'}\rho_{Fm,Fm'}D^{F,f}_{m',\mu}(\delta_{m',\mu+1}-\delta_{m',\mu-1}).\tag{A3}$$

The general solution of Eqs. (17) can be written in a compact form:

$$\delta\rho_{Fm,f\mu}=\sum_{F',f'}\sum_{m',\mu'}T^{F'm',f'\mu'}_{Fm,f\mu}\Omega_2^{f',F'}\times(A^{(2)}_{F'm',f'\mu'}+\Omega_1^{f',F'}A^{(1)}_{F'm',f'\mu'}),\tag{A4}$$

where coefficients $T^{F'm',f'\mu'}_{Fm,f\mu}=(T^{F'-m',f'-\mu'}_{F-m,f-\mu})^*$ are related to $\lambda_{Fm,f\mu}$ and $\Lambda(\delta\rho)_{Fm,f\mu}$, and depend on the Larmor frequency, relaxation rates, detuning, and Rabi frequencies.

[1] A. Omont, Prog. Quantum Electron. **5**, 69 (1977).
[2] W. Happer, Rev. Mod. Phys. **44**, 169 (1972).
[3] B. Decomps, M. Dumont, and M. Ducloy, in *Laser Spectroscopy of Atoms and Molecules*, edited by H. Walther, Topics in Applied Physics Vol. 2 (Springer, Berlin, 1976), p. 284.
[4] M. Ducloy, M. P. Gorza, and B. Decomps, Opt. Commun. **8**, 21 (1973).
[5] *The Hanle Effect and Level-crossing Spectroscopy*, edited by G. Moruzzi and F. Strumia (Plenum, New York, 1991).
[6] W. Gawlik, J. Kowalski, R. Neumann, and F. Träger, Opt. Commun. **12**, 400 (1974).
[7] A. Fischer and I. V. Hertel, Z. Phys. A **304**, 103 (1982).
[8] R. J. McLean, R. J. Ballagh, and D. M. Warrington, J. Phys. B **19**, 3477 (1986).
[9] D. Suter, T. Marty, and H. Klepel, Opt. Lett. **18**, 531 (1993).
[10] T. Yabuzaki, T. Mitsui, and U. Tanaka, Phys. Rev. Lett. **67**, 2453 (1991).
[11] S. Giraud-Cotton, V. P. Kaftandjian, and L. Klein, Phys. Lett. **88A**, 453 (1982).
[12] W. Gawlik, Phys. Lett. **89A**, 278 (1982).
[13] B. Ståhlberg, P. Jungner, T. Fellman, and A. Lindberg, Appl. Phys. B **50**, 547 (1990).
[14] X. Chen, V. L. Telegdi, and A. Weis, Opt. Commun. **74**, 301 (1990).
[15] B. W. Holmes and J. A. R. Griffith, J. Phys. B **28**, 2829 (1995).
[16] H. R. Gray, R. W. Whitley, and C. R. Stroud, Opt. Lett. **3**, 218 (1978).
[17] V. S. Smirnov, A. M. Tumaikin, and V. I. Yudin, Zh. Eksp. Teor. Fiz. **96**, 1613 (1989) [Sov. Phys. JETP **69**, 913 (1989)].
[18] A. Weis, J. Wurster, and S. I. Kanorsky, J. Opt. Soc. Am. B **10**, 716 (1993).
[19] W. Lange and J. Mlynek, Phys. Rev. Lett. **40**, 1373 (1978)
[20] A. Corney, B. P. Kibble, and G. W. Series, Proc. R. Soc. London, Ser. A **293**, 70 (1966).
[21] W. Gawlik and G. W. Series, in *Laser Spectroscopy IV*, edited by H. Walther and K. Rothe (Springer-Verlag, Berlin, 1979), p. 210.
[22] In fact the Gaussian transverse distribution of the incident light beam intensity could lead to a spatial output ring structure as observed by Ståhlberg *et al.* in J. Phys. B **23**, L279 (1990) but this does not significantly change the multipole characteristics.
[23] G. S. Agarwal, *Quantum Statistical Theories of Spontaneous Emission and Their Relation to Other Approaches*, Springer Tracts in Modern Physics Vol. 70 (Springer-Verlag, Berlin, 1974).
[24] A. V. Durrant, J. Phys. B **5**, 133 (1972).
[25] F. Laloë, Ann. Phys. (Paris) **6**, 5 (1971).
[26] J. Zakrzewski and T. Dohnalik, J. Phys. B **16**, 2119 (1983).